Selective Additions of Group 11 and 12 Metal Fragments to the Fe_4C and Fe_5C Units

Joan Camats,[†] Roser Reina,[†] Olga Riba,[†] Oriol Rossell,[†] Miquel Seco,*[,†] Pilar Gómez-Sal,[‡] Avelino Martín,[‡] and Dominique de Montauzon[§]

Departament de Química Inorgànica, Universitat de Barcelona, Martí i Franquès, 1-11, E-08028 Barcelona, Spain, Departamento de Química Inorgánica, Universidad de Alcalá, E-28071 Alcalá de Henares, Spain, and Laboratoire de Chimie de Coordination du CNRS, 205 route de Narbonne, F-31077 Toulouse Cedex, France

Received February 15, 2000

A selective site of interaction has been observed in reacting HgM^+ or $M'PPh_3^+$ (M = $Mo(CO)_3Cp$, $W(CO)_3Cp$; M′ = Au, Cu, Ag) with $[Fe_4C(CO)_{12}\{HgM\}]^-$ to give the mixed-transition-metal clusters $[Fe_4C(CO)_{12}\{HgM\}_2]$ and $[Fe_4C(CO)_{12}\{HgM\}\{M'PPh_3\}]$, respectively. The reaction of $[Fe_5C(CO)_{14}\{HgM\}]^-$ with $M'PPh_3^+$ permits us to obtain the very unstable neutral octanuclear $[Fe_5C(CO)_{14}\{HgM\}\{M'PPh_3\}]$ clusters. The new compounds have been studied by VT-NMR and Mössbauer spectroscopy. The electrochemical behavior of the Fe_4C derivatives has been investigated, and an X-ray crystal structure determination of the complex $[Fe_4C(CO)_{12}\{HgMo(CO)_3Cp\}\{AuPPh_3\}]$ has been carried out.

Introduction

A great number of heterometallic gold− or mercury−iron clusters have been synthesized by the condensation reactions of polyiron anionic carbonyl clusters with the cationic fragments $AuPR_3^+$ and HgM^+ (M = a metal fragment, such as $Mo(CO)_3Cp$).[1] In these species the electrophilic fragments $AuPR_3^+$ and HgM^+ bridge edges or, less frequently, cap faces of the iron polyhedron. The only example in which the gold moiety appears as a terminal ligand is the tetranuclear cluster $[Fe_2Au_2(CO)_8(dppm)]$.[2] The nature of the resulting species is not easy to predict, especially if high-nuclearity clusters are used as building blocks. These generally display different sites of electrophilic attack that usually occur at metal centers with lowest coordination number. The similar ability of the different sites of a given cluster to attach cationic metal fragments has led to the concept of skeletal isomerism,[3] defined by Mingos as those compounds having identical stoichiometry but varying in their skeletal geometry in the solid state.[4]

In the area of iron clusters, the first examples were provided by Shriver, who reported that the trigonal-bipyramidal anionic clusters $[Fe_4M(CO)_{13}]^-$ (M = $AuPPh_3$, HgMe, $HgMo(CO)_3Cp$, $HgFe(CO)_2Cp$) are in equilibrium with a bridged-butterfly form that contains a π-CO ligand.[5] More recently, it has been proved that the complexes $[Fe_4C(CO)_{12}\{AuPEt_3\}_2]$[6] and $[Fe_4C(CO)_{12}\{Au_2(dppm)\}]$[7] also have a different geometry in the solid state. It is remarkable that the reaction of the isolobal species $AuPR_3^+$ and HgM^+ with $[Fe_4C(CO)_{12}]^{2-}$ gives compounds exhibiting different metal cores: the gold atom overbridges the Fe_4C butterfly in the first case,[8] while the mercury atom prefers to bridge one of the two edges defined by wingtip and hinge atoms of the iron butterfly in the second.[9] These results prompted us to extend our studies on the site selectivity of iron anions with group 11 and 12 electrophilic metal fragments in an attempt to compare the site preference of these species and possibly to detect potential competitive processes. This work proved that the starting clusters $[Fe_4C(CO)_{12}]^{2-}$ and $[Fe_5C(CO)_{14}]^{2-}$ allowed the sequential incorporation of metal moieties step by step. It is worth noting here that, in contrast, the anionic mixed gold− or mercury−iron clusters of lower nuclearities, such as $[Fe_2Au(CO)_8(PPh_3)]^-$ or $[Fe_3HgM(CO)_{11}]^-$, are unable to accept additional cationic metal fragments.[10,11] Taking into account the tendency of the carbide clusters to undergo oxidation reactions, we have further extended our studies to the reaction of $[Fe_5C(CO)_{14}\{HgM\}]^-$ [12] with $FeCl_3$ in order to provide a relatively selective synthetic route to clusters of lower nuclearity.

[†] Universitat de Barcelona.
[‡] Universidad de Alcalá.
[§] Laboratoire de Chimie de Coordination du CNRS.

(1) (a) Rosenberg, E.; Hardcastle, K. I. *Comprehensive Organometallic Chemistry II*; Pergamon: Oxford, U.K., 1995; Vol. 10, p 323, and references therein. (b) Salter, I. D. *Comprehensive Organometallic Chemistry II*; Pergamon: Oxford, U.K., 1995; Vol. 10, p 255, and references therein. (c) Ferrer, M.; Reina, R.; Rossell, O.; Seco, M. *Coord. Chem. Rev.* **1999**, *193*−*195*, 619.
(2) Alvarez, S.; Rossell, O.; Seco, M.; Valls, J. Pellinghelli, M. A.; Tiripicchio, A. *Organometallics* **1991**, *10*, 2309.
(3) Rossell, O.; Seco, M.; Segalés, G. In *Metal Clusters in Chemistry*; Braunstein, P., Oro, L., Raithby, P. R., Eds.; Wiley-VCH: Weinheim, Germany, 1999; Vol. 2, p 1053.
(4) Briant, C. E.; Hall, K. P.; Mingos, D. M. *J. Chem. Soc., Chem. Commun.* **1984**, 290.
(5) (a) Horwitz, C. P.; Holt, E. M.; Shriver, D. F. *J. Am. Chem. Soc.* **1985**, *107*, 281. (b) Horwitz, C. P.; Holt, E. M.; Brock, C. P.; Shriver, D. F. *J. Am. Chem. Soc.* **1985**, *107*, 8136. (c) Wang, J.; Sabat, M.; Horwitz, C. P.; Shriver, D. F. *Inorg. Chem.* **1988**, *27*, 552.
(6) Johnson, B. F. G.; Kaner, D. A.; Lewis, J.; Raithby, P. R.; Rosales, M. J. *J. Organomet. Chem.* **1982**, *231*, C59.
(7) Rossell, O.; Seco, M.; Segalés, G.; Johnson, B. F. G.; Dyson, P. J.; Ingham, S. L. *Organometallics* **1996**, *15*, 884.
(8) Bogdan, P. L.; Horwitz, C. P.; Shriver, D. F. *J. Chem. Soc., Chem. Commun.* **1986**, 553.
(9) Reina, R.; Riba, O.; Rossell, O.; Seco, M.; Gómez-Sal, P. Martín, A. *Organometallics* **1997**, *16*, 5113.
(10) Rossell, O.; Seco, M.; Jones, P. G. *Inorg. Chem.* **1990**, *29*, 348.
(11) Reina, R.; Rossell, O.; Seco, M.; de Montauzon, D. Zquiak, R. *Organometallics* **1994**, *13*, 4300.

10.1021/om000151a CCC: $19.00
Publication on Web 07/19/2000

Scheme 1

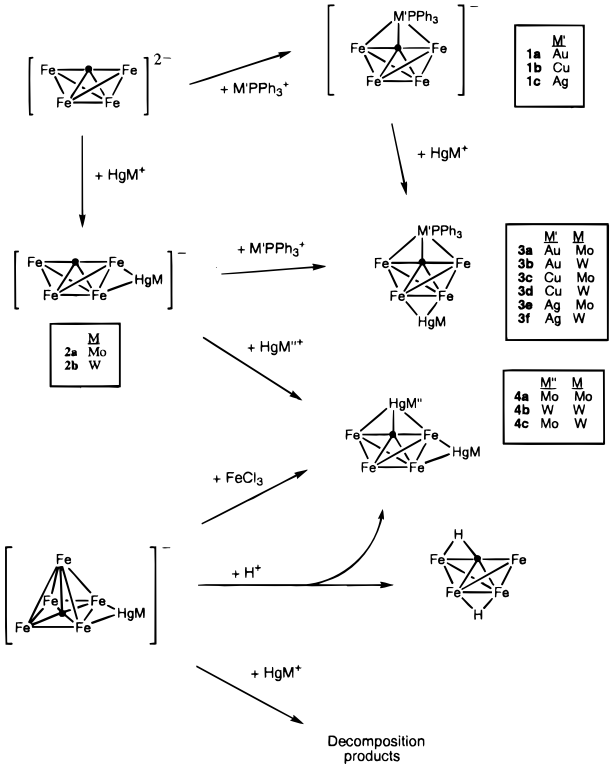

Results and Discussion

Reactions with $[Fe_4C(CO)_{12}]^{2-}$. Prior to this work, $[Fe_4C(CO)_{12}]^{2-}$ had been reacted with $AuPPh_3^+$ and HgM^+ (M = $Mo(CO)_3Cp$, $W(CO)_3Cp$) to give $[Fe_4C(CO)_{12}\{AuPPh_3\}]^-$ (**1**)[8] and $[Fe_4C(CO)_{12}\{HgM\}]^-$ (**2**: **2a**, M = Mo; **2b**, M = W),[9] respectively. In complex **1**, the gold fragment overbridges the Fe_4C butterfly, while the structure of **2a** shows that the HgM^+ moiety bridges one of the two edges defined by wingtip and hinge iron atoms. The different metal core geometries of **1** and **2** account for the tendency of the gold fragment to overlap through its p_x and p_y orbitals with the carbide carbon atom.[13] To test the nucleophilic capability of these species, in the present work, **2a**,**b** were treated with the salts $ClM'PPh_3$ (M′ = Au, Cu, Ag) in CH_2Cl_2 at room temperature, in the presence of $TlBF_4$ as a halide abstractor, and the neutral species $[Fe_4C(CO)_{12}\{\mu\text{-HgM}\}\{\mu\text{-M'PPh}_3\}]$ (**3**) were obtained (Scheme 1).

The ν(CO) IR patterns of these clusters are almost superimposable and show, together with the bands due to the M moieties, the bands of the $Fe_4C(CO)_{12}$ unit, which appear slightly shifted about 15 cm^{-1} to high wavenumbers, indicating a decrease in electron density in the iron atoms. The ^{31}P NMR spectra revealed a signal for the phosphine ligand, which for **3e**,**f** splits into two doublets due to the presence of ^{107}Ag and ^{109}Ag isotopes. It is interesting to note that in VT ^1H and ^{31}P NMR experiments no fluxional behavior was detected in any case.

Along with the signals typical for carbonyl, phenyl, and C_5H_5 groups, the ^{13}C NMR spectra showed the presence of the signal corresponding to the carbido carbon atom at about 440 ppm, which is shifted 25 ppm to lower frequencies relative to the starting compounds **2a**,**b**. This, along with the coupling of the phosphorus atom with the carbon atom ($^2J_{C-P}$ = 56.6 Hz for **3a**,**b**, $^2J_{C-P}$ = 30.8 Hz for **3c**,**d**, and $^2J_{C-P}$(av) = 26.5 Hz, $^1J_{C-^{109}Ag}$(av) = 65.4 Hz, and $^1J_{C-^{107}Ag}$(av) = 56.9 Hz for **3e**,**f**), indicates the strong interaction between the incoming groups and the carbon atom, suggesting that the $M'PPh_3^+$ fragments span the Fe_4C butterfly wingtips. Despite this relevant finding, the final structure of **3** was not evident, if we consider that the Mössbauer spectrum for these clusters consists of two peaks of about the same area, indicating the presence of two kinds of iron atoms in the molecule (vide infra). Obviously, these data are in disagreement with the simple addition of a $M'PPh_3^+$ unit in the Fe_4CM core geometry, so that a correct interpretation requires the assumption that the HgM^+ fragment moves from its original site to another site bridging the hinge of the butterfly.

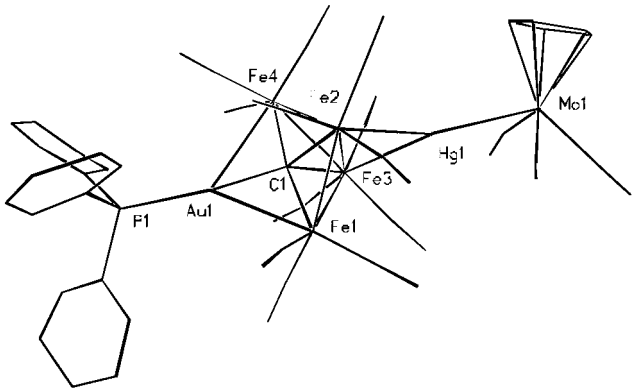

Figure 1. View of a structural line drawing of the cluster $[Fe_4C(CO)_{12}\{\mu\text{-HgMo(CO)}_3Cp\}\{\mu\text{-AuPPh}_3\}]$ (**3a**).

This proposal was confirmed by an attempt of resolution of the structure of the cluster **3a** by an X-ray crystal diffraction study. Unfortunately, the bad quality of the crystal precludes a good refinement (see Experimental Section), but the data available at this moment allow us to resolve the structure and to confirm the most important aspects of the complex. The structure of the compound is shown in Figure 1.

The four Fe atoms define a butterfly arrangement. The Au moiety bridges the two wingtip metal atoms, and the mercury−molybdenum fragment bridges the hinge atoms of the iron skeleton. The carbido carbon atom lies above the center of the Fe(1)−Fe(4) edge. The whole Fe_4C fragment is very similar to that found in other known butterfly systems. The Fe−Fe, Fe−Au, Fe−Hg, and Mo−Hg distances fall in the same range as those found in the related compounds (PPN)$[Fe_4C(CO)_{12}(\mu\text{-H})]$,[14] $[Fe_4C(CO)_{12}(\mu\text{-H})\{\mu\text{-AuPPh}_3\}]$,[6] $[Fe_4C(CO)_{11}(NO)\{\mu\text{-AuPPh}_3\}]$,[15] $[Fe_4CAu_2(CO)_{12}(\mu\text{-dppm})]$,[7] and (PPN)$[Fe_4C(CO)_{12}\{\mu\text{-HgM}\}]$.[9]

It should be noted that the synthesis of **3a**,**b** was alternatively achieved by making **1** react with HgM^+, although it was observed that this process was remarkably slower.

(12) Reina, R.; Riba, O.; Rossell, O.; Seco, M.; Gómez-Sal, P.; Martín, A.; de Montauzon, D. Mari, A. *Organometallics* **1998**, *17*, 4127.
(13) Reina, R.; Rossell, O.; Seco, M.; Segalés, G. *An. Quim. Int. Ed.* **1998**, *94*, 9.
(14) Holt, E. M.; Withmire, K. H.; Shriver, D. F. *J. Organomet. Chem.* **1981**, *213*, 125.
(15) Rossell, O.; Seco, M.; Segalés, G.; Alvarez, S.; Pellinghelli, M. A.; Tiripicchio, A.; de Montauzon, D. *Organometallics* **1997**, *16*, 236.

To detect the preferred site of the iron core to be attacked by the incoming group, **2a**,**b** were treated with HgM^+ species. The reaction was carried out in CH_2Cl_2, at room temperature, affording good yields of the greenish complexes $[Fe_4C(CO)_{12}\{\mu\text{-}HgM(CO)_3Cp\}_2]$ (**4**) (Scheme 1).

We could not grow single crystals of **4a**−**c**, but the geometry of the resulting clusters was proposed on the basis of ^{13}C NMR and ^{57}Fe Mössbauer spectroscopy. The carbido carbon atom appears 15 ppm upfield relative to the starting material, indicating that one of the HgM^+ fragments is overbridging the Fe_4C butterfly. Additionally, compounds of this kind showed in their Mössbauer spectra two peaks with a 3:1 ratio, which is consistent with the proposed skeleton (where the second HgM^+ fragment keeps the original position) if we consider that the iron atoms bonded to the mercury should give almost identical peaks (see Mössbauer Spectroscopy). Interestingly, the new clusters **4** showed fluxional behavior in the temperature range of 250−290 K. Thus, the ^1H NMR spectrum of **4a**,**b** at low temperature displays two signals for the two Cp ligands, which collapse at 285 K.

More interestingly, cluster **4c** shows four signals in the Cp region at low temperature (Figure 2). This implies that a mixture of two isomers is attained in solution: in one, the $HgMo^+$ fragment overbridges the butterfly, while in the other, this position is occupied by the HgW^+ fragment. From Figure 2 it is observed that the central two peaks are distinctly different in intensity. This suggests unequal populations of the two isomers. When the temperature of the solution rises, only two signals appear, indicating a rapid interchange of the mercury fragments. This is not surprising in view of the similar bonding capabilities of the different sites of the iron butterfly core.

Reactions with $[Fe_5C(CO)_{14}\{HgM\}]^-$. In a recent work, we examined the tendency of the $[Fe_5C(CO)_{14}\{HgM\}]^-$ anion to add $AuPPh_3^+$ fragments by giving mixed Au/Hg/Fe clusters.[12] The new cluster $[Fe_5C(CO)_{14}\{HgM(CO)_3Cp\}\{AuPPh_3\}]$ (M = Mo, W) was obtained and fully characterized. Here, we have extended this reaction to the similar copper and silver fragments $M'PPh_3^+$. As expected, the final products $[Fe_5C(CO)_{14}\{HgM(CO)_3Cp\}\{M'PPh_3\}]$ (M = Mo, M′ = Cu (**5a**), Ag (**6a**); M = W, M′ = Cu (**5a**), Ag (**6a**)) are much less stable than the corresponding gold analogues. In all cases, IR and ^1H, ^{13}C, and ^{31}P NMR spectroscopy confirmed the presence of the different ligands in the molecule and FABMS showed the parent molecular peak. The great instability of the new complexes precluded us from obtaining suitable crystals for X-ray diffraction in order to determine unambiguously the coordination mode of the incoming fragment. Attempts to obtain similar complexes containing two HgM^+ fragments were unsuccessful because of the ease of decomposition of the derivatives formed. The fact that the complex $Hg\{M(CO)_3Cp\}_2$ (M = Mo, W) was isolated allows us to propose that a ligand redistribution process takes place during the course of the reaction. Such types of processes are well-documented in the chemistry of mercury.[16]

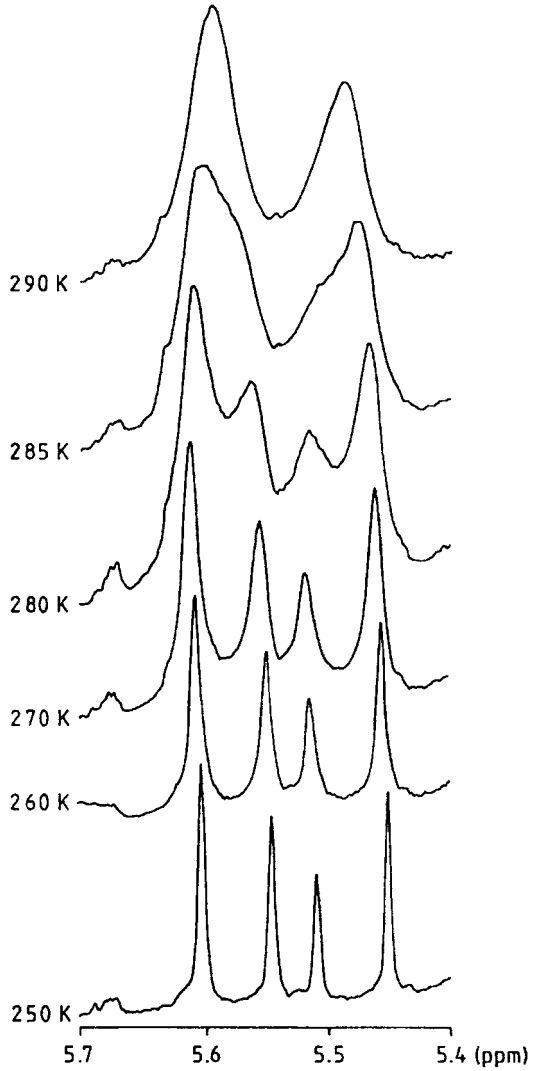

Figure 2. Variable-temperature ^1H NMR spectra in the Cp region of $[Fe_4C(CO)_{12}\{\mu\text{-}HgMo(CO)_3Cp\}\{\mu\text{-}HgW(CO)_3Cp\}]$ (**4c**).

Selective Degradation of $[Fe_5C(CO)_{14}\{HgM\}]^-$. It is well-known that the oxidation reactions of a number of carbide clusters provide selective synthetic routes to clusters of reduced nuclearity. For example, the use of ferric chloride has promoted the degradation of $[Fe_6C(CO)_{16}]^{2-}$ to $[Fe_5C(CO)_{15}]$ or that of $[Fe_5CW(CO)_{17}]^{2-}$ to $[Fe_4CW(CO)_{16}]$.[17] With this in mind, we treated a toluene solution of the $[Fe_5C(CO)_{14}\{HgM\}]^-$ cluster with an aqueous solution of $FeCl_3$ at room temperature for 4 h. Workup of the solution permitted isolation of the lower nuclearity clusters **4a**,**b**, which were obtained after the abstraction of one $Fe(CO)_2$ unit. As anticipated, the yields of this process were lower than those obtained through the reaction of $[Fe_4C(CO)_{12}\{HgM\}]^-$ with HgM^+. For this type of reaction a number of pathways are always available, depending of the type of metal and on the cluster nuclearity. In many examples it has been invoked that the resulting cluster comes from the first degradation of the starting cluster followed by the recombination of the fragments during the course of the reaction. It is remarkable that we have achieved a

(16) Rosenberg, E.; Wang, J. *Organometallics* **1988**, *7*, 1093 and references therein.

(17) Tachikawa, M.; Geerts, R. L.; Muetterties, E. L. *J. Organomet. Chem.* **1981**, *213*, 11.

Table 1. ^{57}Fe Mössbauer Hyperfine Parameters (at 80 K) for Compounds 3c and 4a,c

compd	site	IS[a] (δ), mm s^{-1}	QS (Δ), mm s^{-1}	line width, mm s^{-1}	rel area, %
3c	Fe(1,4)	−0.06	0.93	0.14	47
	Fe(2,3)	0.06	0.77	0.14	53
4a	Fe(1,2,4)	0.04	0.73	0.12	80
	Fe(3)	−0.13	0.76	0.12	20
4c	Fe(1,2,4)	0.05	0.71	0.12	76
	Fe(3)	−0.13	0.72	0.12	24

[a] Isomer shift values are referred to metallic iron at room temperature.

third route to **4a**,**b** through the protonation of $[Fe_5C(CO)_{14}\{HgM\}]^-$ (see Scheme 1). Such reaction types are in general difficult to carry out because of the instability of the hydride derivatives formed. Although several examples of straightforward protonation reactions yield hydrido clusters of unchanged nuclearity, the protonation reaction more frequently leads to species of different nuclearity. This is indeed the case here. In fact, the protonation of $[Fe_5C(CO)_{14}\{HgM\}]^-$ with HBF_4 in CH_2Cl_2 at room temperature afforded **4** and the dihydride $[Fe_4C(CO)_{12}(H)_2]$ (^{1}H NMR (CD_2Cl_2) δ −1.30, −27.95 ppm), which had been previously reported by Muetterties in reacting $[Fe_5C(CO)_{14}]^{2-}$ and HCl.[18] In conclusion, although the mercury−molybdenum/tungsten pentairon carbide proved to be a good nucleophile toward various reagents, the instability of the resulting compounds makes their characterization difficult and in some cases precludes their isolation.

Mössbauer Spectroscopy. The derived spectral hyperfine parameters for compounds **3c** and **4a**,**c** are given in Table 1.

Compound **3c**, in agreement with its X-ray structure, shows two chemically inequivalent iron sites: the two wingtip Fe(1,4) atoms and the two backbone Fe(2,3) atoms. The Mössbauer spectrum is successfully fitted with two symmetric quadrupole doublets with an area ratio of approximately 1:1. The doublet assigned to the backbone iron atoms has the smallest quadrupole splitting, the largest of which is observed for the wingtip iron atoms, indicating that their electronic environment is more distorted. The isomer shift of Fe(2,3) atoms is more positive than that of Fe(1,4), which indicates that the 4s electron density at the iron nucleus of the former is less than for the latter.[19] This fact could be related to the high electrophilic character attributable to the HgM^+ compared with that of the $M'PPh_3^+$ fragment and corroborates well with the ν(CO) shifts observed in IR spectra of each type of iron carbonyl compound.[8−12,15,20−22]

The ^{57}Fe Mössbauer spectra for complexes **4a**,**c** also show two chemically inequivalent iron sites, where the ratio of the areas is approximately 3:1. This suggests that the coordination of the second fragment of HgM^+ makes the three iron atoms indistinguishable for Mössbauer spectroscopy.[23] For both compounds the doublet with the smallest isomer shift corresponds to the iron atom that is not coordinated to the mercury fragment, this assignment being supported by the smaller coordination number of the iron site, as expected.[19b] Finally, the similar quadrupole splitting values may indicate a comparable electronic environment around each iron site.

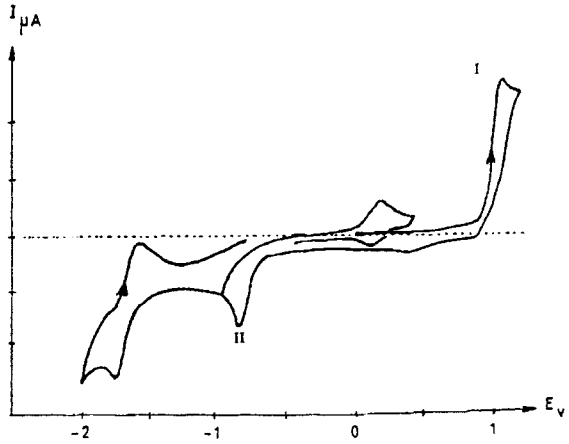

Figure 3. Ambient-temperature cyclic voltammogram of $[Fe_4C(CO)_{12}\{\mu\text{-}HgMo(CO)_3Cp\}\{\mu\text{-}AuPPh_3\}]$ (**3a**) in CH_2Cl_2 measured at a platinum-bead electrode at a scan rate of 0.1 V s^{-1}.

Table 2. Electrochemical Processes for Compounds 3a−f and 4a−c in CH_2Cl_2−0.1 M Bu_4NBF_4 at 0.1 V s^{-1}

compd	oxidn (I) $E_{p,a}$, V	redn (II) $E_{p,c}$, V
3a[a]	1.08	−0.83
3b[a]	1.07	−0.86
3c	1.20	−0.66
3d	1.17	−0.68
3e	1.32	−0.68
3f	1.32	−0.75
4a	1.30	−0.46
4b	1.36	−0.50
4c	1.28	−0.48

[a] For these complexes a Pt working electrode was used.

Electrochemical Study of the Compounds $[Fe_4C(CO)_{12}\{\mu\text{-}HgM\}\{\mu\text{-}M'PPh_3\}]$ (3), $[Fe_4C(CO)_{12}\{\mu\text{-}HgM\}_2]$ (4a,b), and $[Fe_4C(CO)_{12}\{\mu\text{-}HgMo(CO)_3Cp\}\{\mu\text{-}HgW(CO)_3Cp\}]$ (4c). Only studies on Fe_4 derivatives will be reported, given that Fe_5 derivatives were extremely unstable in solution.

$[Fe_4C(CO)_{12}\{\mu\text{-}HgM\}\{\mu\text{-}M'PPh_3\}]$ (3). The electrochemical properties of the title compounds were studied in the electroactivity range of the solvent (CH_2Cl_2), to compare their electrochemical behavior with that of related systems. A cyclic voltammogram of $[Fe_4C(CO)_{12}\{\mu\text{-}HgMo(CO)_3Cp\}\{\mu\text{-}AuPPh_3\}]$ is displayed in Figure 3 as a representative of all of them.

The voltammograms of these neutral compounds show two main electrode processes: (i) an irreversible oxidation wave (I) and (ii) an irreversible reduction step (II). Data for these processes are summarized in Table 2. Two other waves, an oxidation around 0.3 V and a reduction around −1.5 V, are assigned to the intermediate species $[Fe_4C(CO)_{12}\{\mu\text{-}M'PPh_3\}]^-$.[24]

(18) Tachikawa, M.; Muetterties, E. L. *J. Am. Chem. Soc.* **1980**, *102*, 4541.

(19) (a) Benson, C. G.; Long, G. J.; Bradley, J. S.; Kolis, J. W.; Shriver, D. F. *J. Am. Chem. Soc.* **1986**, *108*, 1898. (b) Buhl, M. L.; Long, G. J.; O'Brien, J. F. *Organometallics* **1993**, *12*, 1902.

(20) Reina, R,; Rossell, O.; Seco, M. *J. Organomet. Chem.* **1990**, *398*, 285.

(21) Rossell, O.; Seco, M.; Reina, R. *Organometallics* **1994**, *13*, 2127.

(22) Johnson, B. F. G.; Kaner, D. A.; Lewis, J.; Rosales, M. J. *J. Organomet. Chem.* **1982**, *238*, C73.

(23) This fact has been previously observed for the unreported Mössbauer spectrum of $(PPN)[Fe_4C(CO)_{12}\{\mu\text{-}HgMo(CO)_3Cp\}]$: Riba, O. Graduate Thesis, Universitat de Barcelona, 1997.

(24) Riba, O. Unpublished results.

In the oxidation study controlled-potential coulometry at +1.0 V required 1 faraday/mol and resulted in the formation of a cationic radical which decomposes further. The extra height of this wave is thought to be due to adsorption problems. The proposed mechanism based on the data found for $[Fe_4C(CO)_{12}\{\mu\text{-HgM}\}]$[9] is shown in eqs 1−3.

$$[Fe_4C(CO)_{12}\{HgM\}\{M'PPh_3\}] \rightleftharpoons [Fe_4C(CO)_{12}\{HgM\}\{M'PPh_3\}]^{\bullet+} + 1e^- \quad (1)$$

$$[Fe_4C(CO)_{12}\{HgM\}\{M'PPh_3\}]^{\bullet+} \rightarrow [Fe_4C(CO)_{12}\{HgM\}]^{\bullet} + [M'PPh_3]^+ \quad (2)$$

$$[Fe_4C(CO)_{12}\{HgM\}]^{\bullet} \rightarrow \text{decomposition} \quad (3)$$

A controlled-potential electrolysis is run at −1.0 V, showing that two electrons are exchanged for the reduction process (II). The resulting dianion is not very stable and decomposes according to reactions 4 and 5.

$$[Fe_4C(CO)_{12}\{HgM\}\{M'PPh_3\}] + 2e^- \rightleftharpoons [Fe_4C(CO)_{12}\{HgM\}\{M'PPh_3\}]^{2-} \quad (4)$$

$$[Fe_4C(CO)_{12}\{HgM\}\{M'PPh_3\}]^{2-} \rightarrow [Fe_4C(CO)_{12}\{M'PPh_3\}]^- + Hg + M^- \quad (5)$$

The IR spectrum of the resulting solution showed bands attributable to $[Fe_4C(CO)_{12}\{\mu\text{-M}'PPh_3\}]^-$ and M^- by comparison with the authentic samples. Moreover, silver complexes show two extra waves corresponding to $[Fe_4C(CO)_{12}\{\mu\text{-HgM}\}]^-$, supposedly due to the higher instability of these neutral compounds.

$[Fe_4C(CO)_{12}\{\mu\text{-HgM}\}_2]$ (4a,b) and $[Fe_4C(CO)_{12}\{\mu\text{-HgMo(CO)}_3\text{Cp}\}\{\mu\text{-HgW(CO)}_3\text{Cp}\}]$ (4c). The electrochemical properties of the neutral mercury derivatives were studied using CH_2Cl_2 as a solvent. A typical voltammogram run at 0.1 V s^{-1} shows an irreversible oxidation around +1.3 V and one irreversible reduction around −0.5 V (data in Table 2). For both processes passivation phenomena were observed, precluding a further study for the oxidation process. The reduction was less problematic, and a controlled-potential electrolysis was run at −0.55 V for compound **4a**, showing that one electron is exchanged but the anionic radical obtained decomposes very quickly. We propose the mechanism

$$[Fe_4C(CO)_{12}\{HgM\}_2] + e^- \rightleftharpoons [Fe_4C(CO)_{12}\{HgM\}_2]^{\bullet-} \quad (6)$$

$$[Fe_4C(CO)_{12}\{HgM\}_2]^{\bullet-} \rightarrow [Fe_4C(CO)_{12}\{HgM\}]^- + HgM_2 + \ldots \quad (7)$$

The nature of those final products was detected by IR and cyclic voltammetry. Bearing all this in mind, we can conclude that all the neutral compounds easily lose an electrophilic fragment, giving generally irreversible reductions. This behavior has also been observed for other mercury−iron clusters.[9,11,15] Additionally, irreversible oxidations at greater anodic potential have also been observed for high-nuclearity clusters such as $(NEt_4)[Fe_5C(CO)_{14}\{\mu\text{-HgM}\}]$[12] and $(NEt_4)[Fe_6C(CO)_{16}\{\mu\text{-HgM}\}]$,[15] while the smaller clusters $(PPN)[Fe_4C(CO)_{12}\{\mu\text{-HgM}\}]$,[9] $(PPN)[Fe_4C(CO)_{12}\{\mu\text{-AuPPh}_3\}]$,[24] and $(PPh_4)[Fe_3(CO)_{11}\{\mu\text{-HgM}\}]$[11] show reversible oxidations at lower anodic potentials.

Experimental Section

All manipulations were performed under an atmosphere of prepurified N_2 with standard Schlenk techniques, and all solvents were distilled from appropriate drying agents. Elemental analyses of C and H were carried out at the Unitat de Cromatografia i Microanàlisi del Servei Científico-Tècnic de la Universitat de Barcelona. Infrared spectra were recorded in CH_2Cl_2 solutions on a FT-IR 520 Nicolet spectrophotometer. ^1H, $^{13}C\{^1H\}$, and $^{31}P\{^1H\}$ NMR spectra were obtained on Bruker DRX 250, Varian Unity 300, and Varian XL-500 spectrometers (δ(TMS) 0.0 ppm and δ(85% H_3PO_4) 0.0 ppm). FABMS was recorded on a Fisons VG Quattro spectrometer with CH_2Cl_2 as solvent. The compounds $ClHgM(CO)_3Cp$ (M = Mo, W),[25] $ClAuPPh_3$,[26] $IMPPh_3$ (M = Cu,[27] Ag[28]), and $(NEt_4)[Fe_5C(CO)_{14}\{HgM(CO)_3Cp\}]$ (M = Mo, W)[12] were synthesized as previously described.

Synthesis of $[Fe_4C(CO)_{12}\{\mu\text{-HgM}\}\{\mu\text{-AuPPh}_3\}]$ (M = Mo(CO)$_3$Cp (3a), W(CO)$_3$Cp (3b)). Details of the synthesis of **3a** also apply to **3b**. To a CH_2Cl_2 solution of $(PPN)[Fe_4C(CO)_{12}\{\mu\text{-HgMo(CO)}_3Cp\}]$ (0.35 g, 0.22 mmol in 20 mL) was added $ClAuPPh_3$ (0.11 g, 0.22 mmol) and $TlBF_4$ (0.06 g, 0.22 mmol) at room temperature. The reaction was finished after 20 min, and the color changed from brown to green. The addition of diethyl ether (50 mL) caused the precipitation of PPNCl, which was filtered off. Then, the solution was evaporated to dryness and the residual solid was extracted with 10 mL of toluene. After the solution was layered with hexane (10 mL) and was cooled overnight (−30 °C), green crystals of $[Fe_4C(CO)_{12}\{\mu\text{-HgMo(CO)}_3Cp\}\{\mu\text{-AuPPh}_3\}]$ were obtained: 0.20 g (63% yield). IR (CH_2Cl_2, cm^{-1}): ν(CO) stretch 2064 w, 2022 vs, 1992 vs, 1968 m, sh, 1914 m, 1889 m. ^1H NMR (295 K, CD_2Cl_2, δ (ppm)): 7.6−7.5 (m, 15H, $P(C_6H_5)_3$), 5.4 (s, 5H, C_5H_5). ^{13}C NMR (295 K, CD_2Cl_2, δ (ppm)): 441.7 (d, C, $^2J_{C-P}$ = 56.6 Hz), 216.8 (s, CO), 212.3 (s, CO), 209.2 (s, CO), 134.3−126.5 (m, C_6H_5), 89.1 (s, C_5H_5). ^{31}P NMR (295 K, CH_2Cl_2, δ (ppm)): 40.4 (s, $P(C_6H_5)_3$). FABMS (*m*/*z*): (M^-) 1477, (M − CO) 1448. Anal. Calcd: C, 31.71; H, 1.35. Found: C, 31.81; H, 1.38. Yield for **3b**: 0.18 g, 54%. IR (CH_2Cl_2, cm^{-1}): ν(CO) stretch 2063 w, 2022 vs, 1993 vs, 1966 m, sh, 1905 m, 1883 m. ^1H NMR (295 K, CD_2Cl_2, δ (ppm)): 7.6−7.5 (m, 15H, $P(C_6H_5)_3$), 5.5 (s, 5H, C_5H_5). ^{13}C NMR (295 K, CD_2Cl_2, δ (ppm)): 441.8 (d, C, $^2J_{C-P}$ = 56.6 Hz), 219.6 (s, CO), 217.2 (s, CO), 215.2 (s, CO), 213.8 (s, CO), 212.3 (s, CO), 134.3−129.5 (m, C_6H_5), 87.7 (s, C_5H_5). ^{31}P NMR (295 K, CH_2Cl_2, δ (ppm)): 37.8 (s, $P(C_6H_5)_3$). FABMS (*m*/*z*): (M^-) 1565, (M − CO) 1537. Anal. Calcd: C, 29.93; H, 1.28. Found: C, 30.94; H, 1.30.

Synthesis of $[Fe_4C(CO)_{12}\{\mu\text{-HgM}\}\{\mu\text{-CuPPh}_3\}]$ (M = Mo(CO)$_3$Cp (3c), W(CO)$_3$Cp (3d)). The general procedure described above also applies for **3c**,**d**, but in this case a longer reaction time was needed (1 h). Yield for **3c**: 0.21 g, 62%. IR (CH_2Cl_2, cm^{-1}): ν(CO) stretch 2055 w, 2017 vs, 1991 vs, 1968 sh, 1916 m, 1889 m. ^1H NMR (295 K, CD_2Cl_2, δ (ppm)): 7.5−7.3 (m, 15H, $P(C_6H_5)_3$), 5.4 (s, 5H, C_5H_5). ^{13}C NMR (295 K, CD_2Cl_2, δ (ppm)): 441.7 (d, C, $^2J_{C-P}$ = 30.8 Hz), 215.7 (s, CO), 214.4 (s, CO), 213.7 (s, CO), 211.6 (s, CO), 134.4−129.3 (m, C_6H_5), 89.1 (s, C_5H_5). ^{31}P NMR (295 K, CH_2Cl_2, δ (ppm)): 10.2 (s, $P(C_6H_5)_3$). FABMS (*m*/*z*): (M − CO) 1315. Anal. Calcd: C, 34.86; H, 1.49. Found: C, 34.96; H, 1.51. Yield for **3d**: 0.19 g, 53%. IR (CH_2Cl_2, cm^{-1}): ν(CO) stretch 2055 w, 2018 vs, 1991 vs, 1967 sh, 1909 m, 1885 m. ^1H NMR (295 K, CD_2Cl_2, δ

(25) Mays, M. J.; Robb, J. D. *J. Chem. Soc. A* **1968**, 329.
(26) Kowala, C.; Swan, J. M. *Aust. J. Chem.* **1966**, *19*, 547.
(27) Kauffman, B. B.; Teter, L. A. *Inorg. Synth.* **1963**, *7*, 9.
(28) Teo, B. K.; Calabrase, J. *Inorg. Chem.* **1976**, *15*, 2474.

(ppm)): 7.6−7.5 (m, 15H, $P(C_6H_5)_3$), 5.5 (s, 5H, C_5H_5). ^{13}C NMR (295 K, CD_2Cl_2, δ (ppm)): 441.7 (d, C, $^2J_{C-P}$ = 30.9 Hz), 214.3 (m, CO), 211.6 (s, CO), 134.1−125.6 (m, C_6H_5), 87.7 (s, C_5H_5). ^{31}P NMR (295 K, CH_2Cl_2, δ (ppm)): 9.2 (s, $P(C_6H_5)_3$). FABMS (*m*/*z*): (M^-) 1431, (M − CO) 1404. Anal. Calcd: C, 32.72; H, 1.40. Found: C, 32.74; H, 1.44.

Synthesis of $[Fe_4C(CO)_{12}\{\mu\text{-HgM}\}\{\mu\text{-AgPPh}_3\}]$ (M = Mo(CO)$_3$Cp (3e), W(CO)$_3$Cp (3f)). The general procedure described above also applies for **3e**,**f**, but in this case 2 h was needed to complete the reaction and the Schlenk was kept out of the light in order to avoid silver deposition. Yield for **3e**: 0.26 g, 68%. IR (CH_2Cl_2, cm^{-1}): ν(CO) stretch 2055 w, 2022 vs, 1991 vs, 1912 m, 1890 m. ^1H NMR (295 K, CD_2Cl_2, δ (ppm)): 7.6−7.5 (m, 15H, $P(C_6H_5)_3$), 5.4 (s, 5H, C_5H_5). ^{13}C NMR (295 K, CD_2Cl_2, δ (ppm)): 436.6 (dd, C, $^1J_{C-^{109}Ag}$ = 66.7 Hz, $^1J_{C-^{107}Ag}$ = 57.2 Hz, $^2J_{C-P}$ = 28.0 Hz), 215.1 (s, CO), 211.9 (s, CO), 134.2−125.6 (m, C_6H_5), 89.1 (s, C_5H_5). ^{31}P NMR (295 K, CH_2Cl_2, δ (ppm)): 17.8 (dd, $P(C_6H_5)_3$, $^1J_{P-^{109}Ag}$ = 614.7 Hz, $^1J_{P-^{107}Ag}$ = 532.6 Hz). FABMS (*m*/*z*): (M^-) 1387, (M − CO) 1360. Anal. Calcd: C, 33.75; H, 1.44. Found: C, 33.81; H, 1.46. Yield for **3f**: 0.20 g, 49%. IR (CH_2Cl_2, cm^{-1}): ν(CO) stretch 2055 w, 2020 vs, 1989 vs, 1907 m, 1887 m. ^1H NMR (295 K, CD_2Cl_2, δ (ppm)): 7.6−7.5 (m, 15H, $P(C_6H_5)_3$), 5.5 (s, 5H, C_5H_5). ^{13}C NMR (295 K, CD_2Cl_2, δ (ppm)): 436.8 (dd, C, $^1J_{C-^{109}Ag}$ = 64.1 Hz, $^1J_{C-107Ag}$ = 56.6 Hz, $^2J_{C-P}$ = 25.1 Hz), 215.1 (m, CO), 211.9 (s, CO), 134.3−125.6 (m, C_6H_5), 87.7 (s, C_5H_5). ^{31}P NMR (295 K, CH_2Cl_2, δ (ppm)): 17.8 (dd, $P(C_6H_5)_3$, $^1J_{P-^{109}Ag}$ = 612.4 Hz, $^1J_{P-^{107}Ag}$ = 530.9 Hz). FABMS (*m*/*z*): (M^-) 1475, (M − CO) 1449. Anal. Calcd: C, 31.73; H, 1.36. Found: C, 31.81; H, 1.41.

Synthesis of $[Fe_4C(CO)_{12}\{\mu\text{-HgM}\}_2]$ (M = Mo(CO)$_3$Cp (4a), W(CO)$_3$Cp (4b)). Method A. Details of the synthesis of **4a** also apply to **4b**. Solid $ClHgMo(CO)_3Cp$ (0.07 g, 0.15 mmol) and $TlBF_4$ (0.043 g, 0.15 mmol) were added to a solution of $(PPN)[Fe_4C(CO)_{12}\{\mu\text{-HgMo(CO)}_3Cp\}]$ (0.23 g, 0.15 mmol) in CH_2Cl_2 (15 mL) at room temperature. Over 1 h the color changed from brown to olive green. The solution was stirred for 2 h, filtered through Celite, and layered with diethyl ether (10 mL). After the mixture was cooled to −30 °C overnight, dark green crystals of $[Fe_4C(CO)_{12}\{\mu\text{-HgMo(CO)}_3Cp\}_2]$ were obtained (yield 0.14 g, 66%). IR (CH_2Cl_2, cm^{-1}): ν(CO) stretch 2070 w, 2032 vs, 2026 vs, 2005 s, 1989 sh, 1918 m, 1896 m. ^1H NMR (295 K, CD_2Cl_2, δ (ppm)): 5.5 (s, 5H, C_5H_5). ^{13}C NMR (295 K, CD_2Cl_2, δ (ppm)): 456.5 (s, C), 229.9 (s, CO), 215.1 (s, CO), 211.8 (m, CO), 209.8 (m, CO), 89.1 (s, C_5H_5). FABMS (*m*/*z*): (M^-) 1464, (M − CO) 1436. Anal. Calcd: C, 23.79; H, 0.68. Found: C, 23.79; H, 0.69. Yield for **4b**: 0.21 g. 66%. IR (CH_2Cl_2, cm^{-1}): ν(CO) stretch 2070 w, 2033 vs, 2025 vs, 2007 s, 1990 sh, 1917 m, 1880 m. ^1H NMR (295 K, CD_2Cl_2, δ (ppm)): 5.6 (s, 5H, C_5H_5). ^{13}C NMR (295 K, CD_2Cl_2, δ (ppm)): 455.5 (s, C), 218.7 (s, CO), 215.0 (s, CO), 214.3 (m, CO), 212.6 (m, CO), 211.8 (m, CO), 207.2 (s, CO), 87.8 (s, C_5H_5). FABMS (*m*/*z*): (M^-) 1639, (M − CO) 1611. Anal. Calcd: C, 21.24; H, 0.61. Found: C, 21.25; H, 0.62.

Method B. Details for the synthesis of **4b** also apply to **4a**. To a suspension of $(NEt_4)[Fe_5C(CO)_{14}\{\mu\text{-HgW(CO)}_3Cp\}]$ (0.76 g, 0.56 mmol) in toluene (60 mL) at room temperature was added via syringe aqueous ferric chloride solution (0.46 g, 1.69 mmol in 3 mL of H_2O). The two-layer system was stirred vigorously for 4 h. The green-brown toluene layer was collected, dried with anhydrous Na_2SO_4, and filtered through Celite. The solid obtained by removal of the solvent under reduced pressure was dissolved in the minimum amount of CH_2Cl_2 and layered with hexanes (ca. 2 mL). Dark green crystals were obtained after 72 h at −30 °C (0.23 g, 25%). Yield for **4a**: 0.21 g, 24%.

Synthesis of $[Fe_4C(CO)_{12}\{\mu\text{-HgMo(CO)}_3Cp\}\{\mu\text{-HgW(CO)}_3Cp\}]$ (4c). Solid $ClHgW(CO)_3Cp$ (0.13 g, 0.22 mmol) and $TlBF_4$ (0.065 g, 0.22 mmol) were added to a solution of $(PPN)[Fe_4C(CO)_{12}\{\mu\text{-HgMo(CO)}_3Cp\}]$ (0.35 g, 0.22 mmol) in CH_2Cl_2 (20 mL). The resulting solution was stirred at room temperature for 4 h, and then more $ClHgW(CO)_3Cp$ (0.06 g, 0.11 mmol) and $TlBF_4$ (0.032 g, 0.11 mmol) were added and the solution was stirred for a further 45 min. After this time, $ClHgW(CO)_3Cp$ (0.06 g, 0.11 mmol) and $TlBF_4$ (0.032 g, 0.11 mmol) were added again and the stirring was continued for 30 min. Then, the solution was filtered through Celite, layered with diethyl ether (10 mL), and cooled overnight. Dark green crystals of $[Fe_4C(CO)_{12}\{\mu\text{-HgMo(CO)}_3Cp\}\{\mu\text{-HgW(CO)}_3Cp\}]$ were obtained (yield 0.21 g, 60%). IR (CH_2Cl_2, cm^{-1}): ν(CO) stretch 2071 w, 2032 vs, 2026 vs, 2005 s, 1987 sh, 1910 m, 1892 m. ^1H NMR (295 K, CD_2Cl_2, δ (ppm)): 5.6 (s, 5H, $HgW(CO)_3(C_5H_5)$), 5.5 (s, 5H, $HgMo(CO)_3(C_5H_5)$). ^{13}C NMR (295 K, CD_2Cl_2, δ(ppm)): 215.0 (br, CO), 211.7 (br, CO), 209.7 (br, CO), 89.2 (s, $HgMo(CO)_3(C_5H_5)$), 87.8 (s, $HgW(CO)_3(C_5H_5)$). FABMS (*m*/*z*): (M^-) 1550, (M − CO) 1522. Anal. Calcd: C, 22.45; H, 0.64. Found: C, 22.51; H, 0.65.

Synthesis of $[Fe_5C(CO)_{14}\{\mu\text{-HgM}\}\{\mu\text{-CuPPh}_3\}]$ (M = Mo(CO)$_3$Cp (5a), W(CO)$_3$Cp (5b)). Details for the synthesis of **5b** also apply to **5a**. Solid $ICuPPh_3$ (0.18 g, 0.39 mmol) and $TlBF_4$ (0.11 g, 0.39 mmol) were added to a solution of $(NEt_4)[Fe_5C(CO)_{14}\{\mu\text{-HgW(CO)}_3Cp\}]$ (0.53 g, 0.39 mmol) in CH_2Cl_2 (50 mL) at room temperature. The solution was stirred for 1 h, and 30 mL of diethyl ether was added. After the solution was filtered off, the solvent was evaporated in vacuo and the residue was extracted with toluene (5 × 10 mL). The solution obtained was concentrated to half-volume and layered with 10 mL of hexane. After the mixture was cooled overnight to −30 °C, a mix of brown and yellow particles was obtained (the brown solid corresponded to the desired product, and the yellow solid, HgM_2, came from a partial redistribution reaction of the mercury fragment). This solid was filtered off, and the resulting solution was again layered with 10 mL of hexane. Further cooling caused the precipitation of $[Fe_5C(CO)_{14}\{\mu\text{-HgW(CO)}_3Cp\}\{\mu\text{-CuPPh}_3\}]$ as a brown crystalline solid (0.21 g, 35%). IR (KBr, cm^{-1}): ν(CO) stretch 2068 m, 2025 sh, 2006 vs, 1981 vs, 1942 m, 1911 m, 1883 m, 1838 m, 1820 m. ^1H NMR (295 K, CD_2Cl_2, δ (ppm)): 7.5−7.1 (m, 15H, $P(C_6H_5)_3$), 5.6 (s, 5H, C_5H_5). ^{13}C NMR (295 K, CD_2Cl_2, δ (ppm)): 218.6 (m, CO), 212.7 (s, CO), 133.9−125.6 (m, C_6H_5), 88.2 (s, C_5H_5). ^{31}P NMR (295 K, CH_2Cl_2, δ (ppm)): 11.2 (s, $P(C_6H_5)_3$). FABMS (*m*/*z*): (M^-) 1542, (M − CO) 1514. Anal. Calcd: C, 31.90; H, 1.30. Found: C, 31.09; H, 1.35. Yield for **5a**: 0.18 g, 29%. IR (KBr, cm^{-1}): ν(CO) stretch 2070 m, 2026 sh, 2007 vs, 1987 vs, 1944 m, sh, 1882 s, 1839 m, 1825 m. ^1H NMR (295 K, CD_2Cl_2, δ (ppm)): 7.5−7.1 (m, 15H, $P(C_6H_5)_3$), 5.5 (s, 5H, C_5H_5). ^{13}C NMR (295 K, CD_2Cl_2, δ (ppm)): 218.7 (m, CO), 212.7 (m, CO), 134.1−129.2 (m, C_6H_5), 89.6 (s, C_5H_5). ^{31}P NMR (295 K, CH_2Cl_2, δ (ppm)): 11.4 (s, $P(C_6H_5)_3$). FABMS (*m*/*z*): (M^-) 1453, (M − CO) 1426. Anal. Calcd: C, 33.83; H, 1.37. Found: C, 33.93; H, 1.39.

Synthesis of $[Fe_5C(CO)_{14}\{\mu\text{-HgM}\}\{\mu\text{-AgPPh}_3\}]$ (M = Mo(CO)$_3$Cp (6a), W(CO)$_3$Cp (6b)). The general procedure described above also applies to **6a**,**b**, although all attempts to crystallize these compounds were unsuccessful. In all cases a mixture of the desired product, the anionic starting material, and HgM_2 were obtained along with other decomposition products. Data for **6a** are as follows. IR (KBr, cm^{-1}): ν(CO) stretch 2070 m, 2020 sh, 1997 vs, 1982 vs, 1877 m, 1813 m, 1796 m. ^{31}P NMR (295 K, CH_2Cl_2, δ (ppm)): 9.1 (dd, $P(C_6H_5)_3$, $^1J_{P-^{109}Ag}$ = 366.7 Hz, $^1J_{P-^{107}Ag}$ = 315.4 Hz). FABMS (*m*/*z*): (M^-) 1498. Data for **6b** are as follows. IR (KBr, cm^{-1}): ν(CO) stretch 2069 m, 2020 sh, 1996 vs, 1982 vs, 1870 m, 1843 m, 1815 m. ^{31}P NMR (295 K, CH_2Cl_2, δ (ppm)): 10.2 (dd, $P(C_6H_5)_3$, $^1J_{P-^{109}Ag}$ = 373.7 Hz, $^1J_{P-^{107}Ag}$ = 322.5 Hz). FABMS (*m*/*z*): (M^-) 1587.

Electrochemical Measurements. Electrochemical measurements were carried out with an Electrokemat potentiostat[29] using the interrupt method to minimize the uncompensated resistance (*iR*) drop when the working electrode was

(29) Cassoux, P.; Dartiguepeyron, R.; de Montauzon, D.; Tommasino, J. B.; Fabre, P. L. *Actual. Chim*. **1994**, *1*, 49.

Pt. Electrochemical experiments were performed at room temperature in an airtight three-electrode cell connected to a vacuum argon/N_2 line. The reference electrode consisted of a saturated calomel electrode (SCE) separated from the non-aqueous solutions by a bridge compartment. The counter electrode was a spiral of ca. 1 cm^2 apparent surface area, made of a platinum wire 8 cm in length and 0.5 cm in diameter. The working electrode was Au (0.125 mm diameter) or Pt (1 mm diameter) for cyclic voltammetry or a rotating-disk electrode of Pt of 2 mm diameter for linear voltammetry. For electrolysis a Au wire or a Pt foil was used. $E°'$ values were determined as the average of the cathodic and anodic peak potentials, i.e., $(E_{p,c} + E_{p,a})/2$. The supporting electrolyte (n-$Bu_4N)[BF_4]$ (Aldrich analytical grade) was used as received. Dichloromethane (SDS purex) was freshly distilled over $CaCl_2$ and then over P_2O_5 prior to use. The solutions used during the electrochemical studies were typically 4×10^{-4} M in the organometallic complex and 0.1 M in (n-$Bu_4N)[BF_4]$. Under the same conditions, ferrocene is oxidized at $E°' = 0.42$ V vs SCE and the peak potential separation ΔE is 60 mV.

Mössbauer Measurements. The Mössbauer spectra were recorded in a transmission geometry using driving equipment of constant acceleration provided by a ^{57}Co (50 mCi) source diffused into a Rh matrix and calibrated at room temperature with natural-abundance α-iron foil. The measurements were carried out at 80 K using an MD 306 Oxford cryostat. The spectra were fitted to symmetrical Lorentzian doublets by using standard least-squares computer minimization techniques.[30]

X-ray Structure Determination of 3a. Poor-quality crystals of **3a** were obtained by crystallization from toluene/hexane, and the best of them were selected and mounted on an Enraf-Nonius CAD 4 automatic four-circle diffractometer with graphite-monochromated Mo Kα radiation ($\lambda = 0.710\ 73$ Å). The presence of a large residual of electronic density near Hg (28 e $Å^{-3}$) and Au in the final difference Fourier map informs us about the presence of a serious disorder problem that it is not possible to solve. The R1 factor at this point was 0.2394 for all the observed reflections. Crystallographic and experimental details for the structure are described in the Supporting Information.

Acknowledgment. This work was supported by the DGICYT (Project PB96-0174). We thank Alain Mari for his experimental assistance in the Mössbauer measurements.

Supporting Information Available: Tables giving experimental details of the X-ray structural detemination, final values of atomic coordinates for the non-hydrogen atoms, anisotropic thermal parameters for the non-hydrogen atoms, and all bond distances and angles. Ordering information is given on any current masthead page.

OM000151A

(30) Varret, F. *Proceedings of the International Conference on Mössbauer Effect Application*; Jaipu, India, 1981; Indian National Science Academy: New Delhi, India, 1982.